J. Fluid Mech. (1983), *vol.* 136, *pp.* 85–109
Printed in Great Britain

Trailing vortices in homogeneous and density-stratified media

By TURGUT SARPKAYA
Naval Postgraduate School, Monterey, CA 93940

(Received 15 October 1982 and in revised form 11 July 1983)

Experiments were conducted with three delta wings and two rectangular wings to investigate the evolution of trailing vortices in stratified and unstratified water. The vortex trajectories were determined as a function of the normalized time $V_0 t/b_0$, stratification parameter Nb_0/V_0 and an effective vortex-core size r_c/b_0. The results have shown that the vortices rise only to a finite height as they decay gradually at first and rapidly thereafter under the influence of turbulence, sinusoidal instability, and core bursting. The effect of stratification is to reduce the lifespan of vortices and the maximum height attained by them.

1. Introduction

Vortices and vortex wakes have become a major theme of aerodynamics research since the advent of the large aircraft and the understanding of their evolution required an examination of many fundamental problems in fluid mechanics. Much of the progress made during the past two decades was discussed at the Symposium on Aircraft Wake Turbulence and Its Detection (Olsen, Goldburg & Rogers 1971) and at the Aircraft Wake Vortices Conference (Hallock 1977). Comprehensive reviews of the entire subject have been given by Donaldson & Blanin (1975), Widnall (1975) and Hallock & Eberle (1977).

These studies, as well as numerous others carried out since 1977, have shown that there are several obstacles to the development of a better understanding of the important features of trailing vortices. The principal ones are as follows. (i) *Roll-up process.* The velocity and turbulence distributions at any section behind the wing depend on the wing section, wing tip shape, Reynolds number, wing incidence, and the distance of the station from the wing (see e.g. Panton, Oberkampf & Soskic 1980). The distributions of the initial velocity and turbulence, which influence the roll-up and the decay processes, cannot be changed independently. For example, a change in tip shape changes the core size, as well as the velocity and turbulence distributions. High levels of turbulence result in an increased diffusion of vorticity, which in turn increases the core size. (ii) *Probe sensitivity of the vortices.* Flow-visualization studies suggest that trailing vortices are extremely sensitive to disturbances created by even very small probes or bubbles. This forces one to use non-intrusive means of measurements such as an LDV. Even then, 'vortex wandering' (Baker *et al.* 1974), which makes the vortices appear larger than normal in time-averaged velocity measurements (for vortices generated by a wing in a wind tunnel), or the unsteady nature of the flow (for vortices generated by a wing in a tow basin) makes the mean velocity profiles in the vortices difficult to determine. (iii) *Large-scale instabilities.* The vortices were never observed to decay away owing to viscous and turbulent dissipation, but were always destroyed by either mutual induction instability (Crow

1970) and/or vortex breakdown. The Crow instability grows exponentially, and results either in a linking of the vortex pair into a series of crude vortex rings or in a highly disorganized intermingling of the vortices. Vortex breakdown, whose mathematical details have not yet been adequately treated, rearranges the vortex structure and increases the core size, turbulence, and energy dissipation. Thus it is very difficult to measure accurately the trajectories of the three-dimensional vortices from their creation to their ultimate demise. (iv) *Reynolds number*. Even the highest Reynolds numbers, based on wing chord, reached in wind tunnels or towing basins, are an order of magnitude lower than what is possible for an aircraft. Thus, the scale effects are not easy to assess. Finally, (v) *ambient conditions* such as turbulence and stratification play major roles in the evolution of vortices. The quantification of these effects offers exceedingly complex difficulties.

The majority of the experimental data have been obtained in large-scale atmospheric tests using aircraft (Burnham *et al.* 1978) or from vortex rings (Hecht *et al.* 1980). Flight tests are usually limited in both the quantity and quality of information that can be extracted because of the vagaries of atmospheric flow conditions. Barker & Crow (1977) and Tomassian (1979) have created two-dimensional vortices in a small tank with large circulations and comparably small separations.

Mathematical and numerical dynamic modelling of a two-dimensional vortex pair has been attempted, sometimes with discordant results (Widnall 1975) regarding the vortex spacing, migration speed and the maximum height attained by the vortices. Some of these studies which relate in some way to our study will be highlighted later.

The goal of the present study is to determine the lifespan of three-dimensional trailing vortices, generated by various lifting surfaces in homogeneous and stably stratified water, and to obtain definitive data against which the mathematical models and computational techniques may be checked. Clearly, the Reynolds number in our experiments is lower than one might expect for practical purposes, but the object of the investigation was the understanding of the evolution of the vortices under controlled conditions rather than to provide design data. It is to be hoped that such works will help in the interpretation of the full-scale results and will provide inspiration for the development of improved mathematical models of the flow.

2. Experimental facility and procedure

The experiments were performed in a towing tank. Initially, it had a length of 11 m, a width of 0.91 m, and a depth of 1.52 m. Subsequently, it has been enlarged to $15 \times 1.2 \times 1.83$ m. The back wall of the tank is made of 1.0 cm aluminium plates and reinforced to prevent bulging under hydrostatic pressure. The front wall is fitted with square windows of 2.54 cm, military grade, craze-resistant Plexiglas sheets. Horizontal braces were placed at suitable intervals to reduce lateral deflection.

Vertical and horizontal scales of 1.27 cm increments are marked on the central window. The scales are used to evaluate the position of the vortices and the vertical amplitude of sinusoidal instability, after proper calibration for the refraction and parallax effects.

Two parallel rails are mounted along the bottom of the tank. A carriage rides smoothly on these rails and provides the test body with a constant velocity through the use of an endless cable and a variable-speed motor. The velocity of the model is measured and continuously monitored through the use of a magnetic velocity sensor attached to the carriage. Models reached their terminal velocity in less than 0.2 s. The terminal velocity did not vary more than 0.5 % during a given run. The two rails,

the carriage and the filling pipes are located under a turbulence management system. This system consisted of a 2.54 cm polyurethane foam, sandwiched between two perforated aluminium plates.

The stratification system consisted of a number of tanks and necessary tubes and valves. First brine water of certain salt concentration is prepared in one of these tanks. Then precalculated amounts of brine are added to other tanks, depending on the density gradient desired. The resulting solutions are drained into the tank at a very slow rate (with the help of a cam-timer-operated valve) in the order of increasing density. The filling of the entire test tank required approximately 5 h. Necessary precautions were taken to prevent air entrainment and subsequent bubble generation. Very linear density gradients were obtained, as verified with a fast-response concentration probe which was traversed vertically with the aid of a small motor (approximately 1 h after the filling of the test tank).

Finally, two parallel rails, mounted along the top of the towing tank, and a carriage supported the lights, a camera, and a mirror. This system enabled the photographing of the top view of the trailing vortices at regular intervals. Supplementary description of the equipment and procedure may be found in Sarpkaya & Johnson (1982).

2.1. *Test models*

Five models were used in the experiments. The first three models are delta wings, made of 3 mm thick aluminium with hollow interiors. The first delta wing (delta-1S) had an apex angle of 39.5°, a base width $B = 20$ cm, and an aspect ratio $AR = 1.436$. The second delta wing (delta-2S) had an apex angle of 50°, a base width $B = 12.9$ cm, and an aspect ratio $AR = 1.69$. The pressure side of the leading edges of these models were made razor sharp. The edges of the suction side were bevelled to an angle of 45°. The third delta wing (delta-3R) was identical with the second one, the only difference being in the shape of the edges. In this case, all edges were rounded to a radius of 1.5 mm (half the plate thickness) in order to examine the effect of the edge modification on the longevity of the vortices.

The fourth and fifth models (RP-1 and RP-2) were of rectangular shape, with a NACA-0012 cross-section, and had an aspect ratio $AR = 1.943$ ($B = 17.3$ cm for RP-1 and $B = 11.4$ cm for RP-2). The wing tips were rounded to a radius equal to half the local thickness of the foil. The interior of each model was hollowed and used as a dye reservoir to seed the vortex cores.

Each model cavity was filled with dye prior to the filling of the tank with water. The two holes on the suction side of the rear edges of each model and the third hole in the middle of the upper surface (pressure side of the model) were plugged prior to an experimental run to prevent dye leakage. The dye consisted of milk, ground methylene blue particles, food colouring and the required amounts of ethanol. The density of the mixture was such that the dye was only slightly buoyant relative to its surroundings. Occasionally, Rhodamine WT or B was added into the mixture. The seeding of the vortex cores with this mixture helped to trace the path of the vortices.

In addition to the foregoing, small methylene blue particles (approximately 0.6 mm cubes) were dropped into the homogeneous or stratified water at positions where the trailing vortices rose (i.e. at $\pm\frac{1}{2}b_0$, half the vortex spacing from the axis of the model). These particles sank to the bottom of the basin along a straight vertical path before the start of the experiment. Along the particles' path, methylene blue dissolved from the surface and left a trace in the wake of the sinking particle. The coefficient of diffusion of methylene blue in water or in salt-stratified medium is very small, and dye remains sharp and easily identifiable for a period of about 30 min. The dye streaks

were captured by the vortex pair and deformed according to the local displacement of the fluid. This method made it easier to trace the path of the vortices and of the vortex rings during the later stages of their motion.

The residual velocity in the tank due to convection and previous runs was about 0.2 mm/s at the start of a new run. A thin layer of oil was spread over the free surface to prevent evaporation cooling and thereby to minimize the residual velocities.

The models were mounted in the middle of their bases by means of a streamlined thin vertical support strut (its cross-section was a NACA-0006 foil with a chord length of 13 mm) and set at the desired angle of attack (from $-8°$ to $-12°$). The models were placed at a level 45.7 cm above the foam. As noted earlier, all models were pulled by means of a d.c. motor, pulley and cable system at the desired speed (ranging from 30 to 150 cm/s). Chord-based Reynolds numbers ranged from 4×10^4 to 5×10^5.

The motion of the trailing vortices was recorded on high-speed film at the test section. Each picture included two timers, accurate to 0.01 s, the vertical and horizontal scales on the window and, of course, the side view of the vortices as they rose after formation. The top view of the vortices was photographed with a separate camera. Each experiment was repeated at least twice to ascertain that the results were reproducible. It is important to note that each stratification was used only for one run. All trailing vortices and vortex rings were recorded on film until the time they have completely dissipated. The maximum height measured depends somewhat on the relative position of the plane of observation with respect to the phase of the sinusoidal deformation or of the vortex breakdown. As a result, the last data points exhibited larger scatter.

2.2. *Core size*

The vortices generated by the sharp-edged wings had a larger diameter and relatively rougher surface. The vortices generated by wings with rounded edges had a smaller diameter and smoother surface. It is on the basis of these observations that it was decided to measure the core size as accurately as possible. The use of a non-intrusive technique was necessary since it was impossible to introduce any type of velocity sensor into the vortex core without causing immediate vortex breakdown. For this purpose a mixture of fluorescein and Liquitex Retarding Madium-5447† (resulting in a dough-like substance) was spread over the pressure side of the model and baked for 10 min with a heat lamp. Then the surface was polished with sandpaper. The final thickness of the baked mixture was about 0.2 mm. When the model was set in motion, fluorescein was released from the surface and rolled up into two tight vortices in a short distance.‡ The vortex core appeared as a bright column in water and was photographed with a high-speed camera through the use of quartz lamps, which emit a large amount of ultraviolet light, and a transparent plastic paper with a mm grid engraved on it.

The core measurements were made at angles of attack of $-8°$ and $-12°$ and at model velocities of $U = 0.91$ m/s and $U = 1.37$ m/s, at a distance of *ten chord lengths* downstream from the model. The diameter of the dye column was taken as the initial‖ effective core size. It represented the region containing vorticity, save for the effect

† Available from art shops.

‡ According to Spreiter & Sacks (1951) the vortices are considered to be essentially rolled up in a distance s given by $s/c = 0.36\,(AR/C_L)\,b_0/c$, where c denotes the chord length. For the models used here, s/c ranged from 0.7 to 3, using the C_L values (lift coefficients) given by Hoerner (1958).

‖ Here and throughout the rest of the paper, the conditions prevailing at ten chord lengths are designated as the 'initial' conditions.

of the diffusion of dye over a distance of ten chord lengths. The relationship between this core definition and others, such as the point of maximum velocity or a definition based on equivalent energy in the vortex (Spreiter & Sacks 1951), cannot be deduced from these measurements.

The average of at least five measurements per model yielded $r_e/b_0 = 0.13 \pm 0.02$ for the sharp-edged models and $r_e/b_0 = 0.09 \pm 0.01$ for the wings with rounded edges. The wing shape and the aspect ratio did not have a measurable effect on r_e/b_0. Admittedly, it is very difficult to obtain a precise measurement of r_e and to account for the diffusion of dye over a time period of $10\,c/U$ (0.5–3 s). However, in all cases, r_e did not differ more than about 12% from the average of over five measurements per model.

3. Discussion of results

3.1. *Dimensional analysis*

The dependent parameter of major importance is the displacement H of the vortex in the vertical direction, and it may be expressed as a function of the following independent parameters:

$$H = f(t, U, D, \rho_0, \mathrm{d}\rho/\mathrm{d}y, \nu, B, AR, \alpha, g, r_e), \tag{3.1}$$

in which t represents the time, U the velocity of the model, D the initial depth of the vortex pair, ρ_0 the reference density of water, $\mathrm{d}\rho/\mathrm{d}y$ the linear density gradient, ν the kinematic viscosity of water, B the base width of the model, AR the aspect ratio of the model (here rectangular or triangular lifting surfaces), α the angle of attack, g the gravitational acceleration, and r_e an effective core radius, characterizing the effect of the wing-tip shape in addition to other wing parameters.

The height and width of the test section and the height of the model within it were not included in the foregoing because a detailed analysis, based on ideal vortices, has shown that the velocities induced by the bottom and sidewall image pairs were negligible. The free-surface effects are discussed later.

A dimensional analysis of (3.1) yields

$$\frac{H}{B} = f\left(\frac{Ut}{B}, \frac{D}{B}, \frac{NB}{U}, \frac{U^2}{gB}, \frac{UB}{\nu}, AR, \alpha, \frac{r_e}{B}\right), \tag{3.2}$$

in which

$$N = \left(-\frac{g}{\rho_0}\frac{\mathrm{d}\rho}{\mathrm{d}y}\right)^{\frac{1}{2}} \tag{3.3}$$

and is known as the Brunt-Väisälä frequency.

Equation (3.3) may be recast in terms of the initial separation b_0 of the vortex pair, and the initial mutual-induction velocity V_0 of the vortex pair, by noting that b_0/B and V_0/U are uniquely determined by AR and α for a given wing-tip shape. Thus one has

$$\frac{H}{B_0} = f\left(\frac{V_0 t}{b_0}, \frac{D}{b_0}, \frac{NB_0}{V_0}, \frac{V_0^2}{gb_0}, \frac{V_0 b_0}{\nu}, \frac{r_e}{b_0}\right). \tag{3.4}$$

Experiments were performed with a given body by varying the angle of attack and the speed of the body for a given N. Then H and $b(t)$ were determined from the motion pictures at 0.5 s intervals. Note that $(H, t) = (0, 0)$ and $b(0) = b_0$. The initial migration velocity V_0 was calculated from $H(t)$ by fitting a fourth-order polynomial to the first

five points of the trajectory, where V_0 is simply the coefficient of t. In this investigation V_0 ranged from 1.5 to 5 cm/s.

The b_0/B values are given in table 1. These values are in good agreement with those obtained by Elle (1958). For rectangular wings, b_0/B was found to be nearly equal to $\frac{1}{4}\pi$ (its theoretical value for an elliptically loaded wing).

α\Model	Delta-1S	Delta-2S
$-8°$	0.72	0.71
$-10°$	0.71	0.71
$-12°$	0.70	0.71

TABLE 1. Measured values of b_0/B for two sharp-edged delta-wing models

As to the effect of the wing-tip shape on b_0/B, there is very little data and much disagreement (Hoerner 1958; Bartlett & Vidal 1955; Elle 1958). The vortex height above the leading edge (upper surface) was about the same for rounded and sharp-edged delta wings. However, for sharp-edged delta wings the vortex-centre lines were a little further outwards towards the leading edge relative to those for the rounded delta wing. This observation is in conformity with that of Elle (1958). One would expect that the flow on the upper surface of the rounded edge remains attached until it is at an appreciable angle to the plane of the wing surface. This, in turn, leads to a slightly smaller b_0/B and relatively tighter roll-up of the vortex sheet for wings with rounded edges.

The measurements have shown that the dimensionless parameters V_0^2/gb_0 (a Froude number which ranged from 3×10^{-3} to 3×10^{-2}) and $V_0 b_0/\nu$ (a Reynolds number which ranged from 3500 to 10500) are not important within the range of the parameters encountered in the present experiments. With the foregoing arguments, (3.4) may be written as

$$H^* = f(t^*, D^*, N^*, r^*), \tag{3.5}$$

where $H^* = H/b_0$, $D^* = D/b_0$, $t^* = V_0 t/b_0$, $N^* = Nb_0/V_0$ and $r^* = r_c/b_0$. For sufficiently large values of D^* the free-surface effects become negligible, making H^* dependent only on t^*, N^* and r^*. Whereas the parameters t^* and N^* may be changed independently, r^* is taken as nature provides it. The primary reason for this is that a century of theoretical and experimental aerodynamics research has been incapable of describing the details of the structure of the tip vortex to be used as initial conditions in a viscous solution. It is surprising, but true, that up until recently the importance of the wing-tip shape and its influence upon both the initial tangential velocity profile and the initial turbulence in the vortex has not been fully appreciated. Here we have characterized the said influence in terms of an effective core radius with full awareness of its shortcomings.

3.2. *Trailing vortices in homogeneous fluid*

Figure 1 shows H^* for $D^* = 7.73$ as a function of t^* for the sharp-edged delta wings for representative model velocities and angles of attack. Aside from some minor scatter at large values of t^*, for the reasons cited earlier, the results of the two models compare quite well. Upper solid line represents the trajectory of two inviscid vortices rising in an infinite homogeneous fluid, i.e. $H^* = t^*$ for $D^* = \infty$.

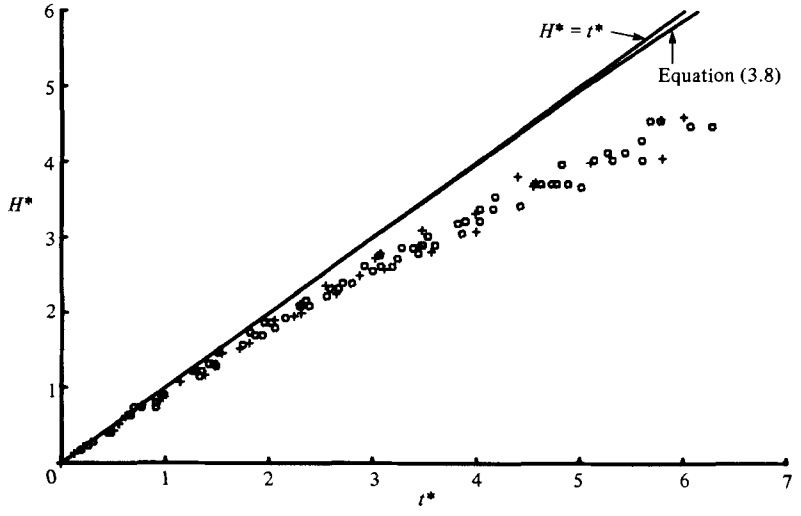

FIGURE 1. Rise of vortices generated by sharp-edged delta wings: +, $AR = 1.436$; ○, $AR = 1.69$.

The trajectories of the ideal line vortices approaching a rigid plane are hyperbolas given by (Lamb 1945)

$$\frac{b_0^2}{(2x)^2}+\frac{b_0^2}{(2y)^2}=1+\frac{b_0^2}{(2D)^2}. \tag{3.6}$$

The coordinate x is along the boundary and y is normal to it. The vortices do not come to the plane surface a distance closer than

$$y_{\min}=\frac{b_0}{2}\left(1+\frac{b_0^2}{(2D)^2}\right)^{-\frac{1}{2}}. \tag{3.7}$$

Also, it is easy to show that t^* is related to H^* by

$$t^*=\frac{1}{2}\left(\frac{m^2}{1+m^2}\right)^2\left(\frac{m^2-1}{m}-\frac{(1+m^2)\eta^2-2}{[(1+m^2)\eta^2-1]^{\frac{1}{2}}}\right), \tag{3.8}$$

where

$$m=2D^*,\quad \eta=y/D,\quad H=D-y,\quad H^*=\tfrac{1}{2}m(1-\eta). \tag{3.9}$$

The lower solid curve in figure 1 represents (3.8) for $D^* = 7.73$. Clearly, the difference between the two solid curves is negligible, showing that the behaviour of vortices starting at a finite depth of $D^* = 7.73$ (as in the present experiments) is not materially different from those starting at an infinite depth. For this reason, the data reported here were obtained with $D^* \geqslant 7.73$, and D^* was eliminated as an independent parameter. It must be noted in passing that the free surface does not behave like a rigid surface when the vortices are allowed to come close to it. The interaction of the trailing vortices or vortex rings, generated at a small finite depth, with the free surface is considerably more complex and will not be discussed here further.

Figure 2 shows a comparison of the data obtained with round- and sharp-edged delta wings with $AR = 1.69$ and $D^* = 7.73$. The solid line represents $H^* = t^*$. Clearly, the smaller the effective core size the larger the value of H^* to which the vortex cores rise. Furthermore, the vortices with smaller core have a longer lifespan.

Representative data obtained with rectangular wings are shown in figure 3. Once

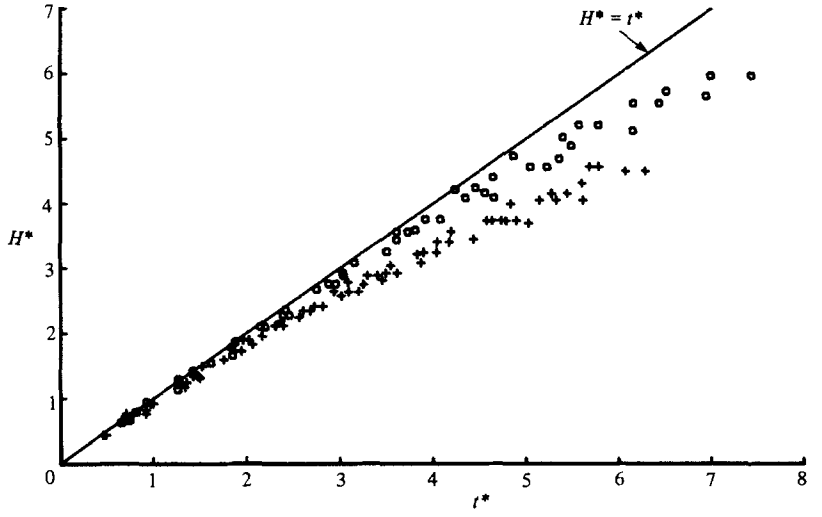

FIGURE 2. Comparison of vortex rise height for delta wings with: ○, rounded tips and +, sharp-edged tips.

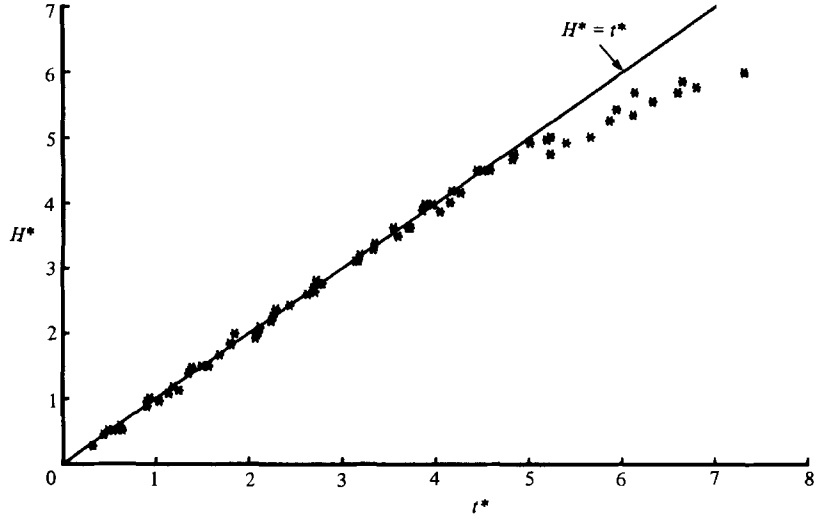

FIGURE 3. The rise of trailing vortices generated by rectangular wings (NACA 0012).

again it is clear that the vortices rise to relatively larger heights when compared with those generated by sharp-edged Delta wings (figure 1).

One is now in a position to determine as to whether the aspect ratio and the model shape and hence their attendant consequences on the roll-up process have any effect on the rise of vortices for a given core size. For this purpose, the data obtained with the rounded delta wing and the rectangular wings are compared in figure 4. It is clear that there is very little difference between the two sets of data. Thus one may conclude tentatively that the aspect ratio and the shape of the model do not materially affect the variation of H^* with t^*. On the other hand, the rounding of the wing tips and the resulting changes in the initial core size and structure of the vortices have profound effects on the rise and ultimate demise of the trailing vortices. Additional

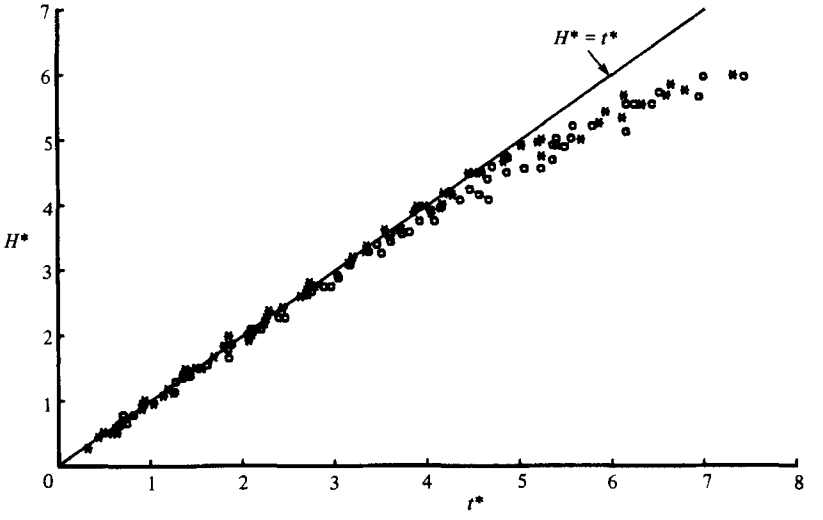

FIGURE 4. Comparison of data obtained with rectangular (NACA 0012) and delta wings with rounded tips: *, NACA 0012; ○, delta-3R.

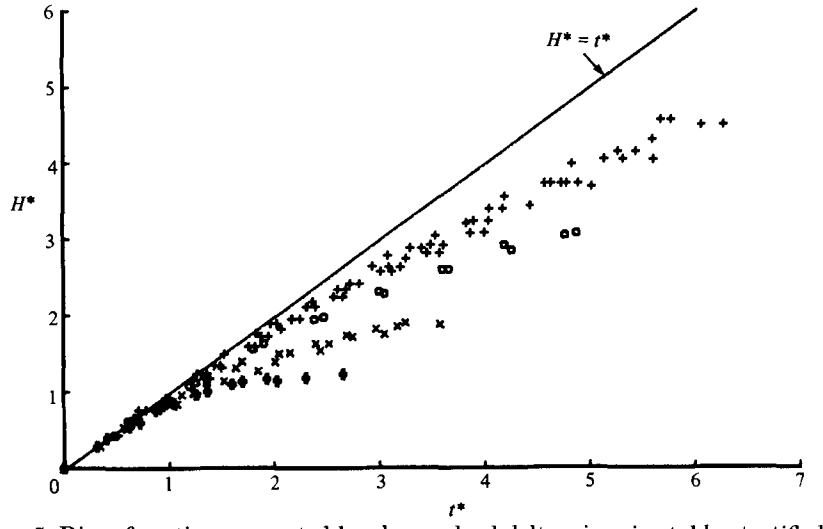

FIGURE 5. Rise of vortices generated by sharp-edged delta wings in stably stratified water for various values of N^*: +, 0; ○, 0.50; ×, 0.75; #, 1.00.

experiments with other shapes of models and wing tips are needed to put the foregoing conclusion on a firmer basis.

3.3. *Trailing vortices in stratified fluid*

The data obtained with sharp-edged delta wings in stratified water are shown in figure 5 for representative values of the stratification parameter N^*. It is important to note that in this set of experiments D^* was chosen larger than 7.73 so as to exclude the effect of free surface and thus concentrate only on the effects of linear stratification. Clearly, the larger the stratification, the smaller the rise of vortices. The vortices continue to ascend slowly until they are completely destroyed by subsequent instability events to be described in §4.2. There is no evidence of acceleration of the

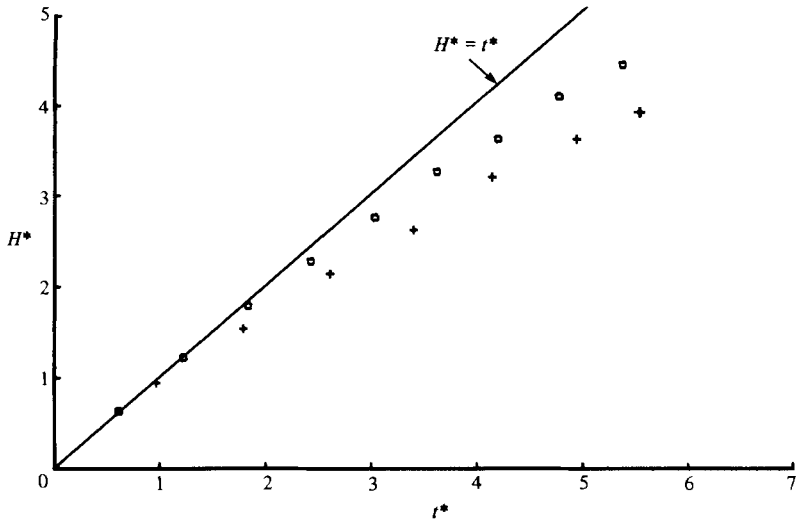

FIGURE 6. The effect of tip shape on the rise of vortices in stratified water: +, (sharp-edged delta wing: delta-2S); ○, (delta wing with rounded tips: delta-3R). $N^* = 0.375$ for both cases.

vortex pair during the course of its rise and demise. The fundamental conclusion to be deduced from figure 5 is that the effect of the stable stratification is to inhibit the rise of the trailing vortices. This is due to a number of reasons such as (i) the increase of the downward buoyant force on the recirculation cell, (ii) the generation of countersign vorticity outside the recirculation cell (a contribution of $-(g/\rho_0)\,\mathrm{d}\rho/\mathrm{d}x$ in the momentum equation), (iii) the decrease in circulation due to the cancellation of vorticity of opposite signs in the overlapping boundaries of the vortex pair, (iv) the enhanced effect of the entrainment and/or detrainment of the recirculation cell, (v) the change of the turbulence structure and hence the eddy diffusion by stratification, and other as yet unknown demise mechanisms associated with stratification.

A series of experiments were conducted with rectangular wings and rounded Delta wings in stratified water. The effect of the reduction of the effective core size on the rise of vortices was quite similar to that in unstratified fluid. Figure 6 shows a comparison of the data obtained with the rounded and sharp-edged Delta wings for $N^* = 0.375$. Clearly, the smaller the core, the larger the rise of vortices. The extensive data obtained with other stratifications yielded the same conclusion.

4. Demise of the trailing vortices

We come now to one of the central questions raised by the experiment: how are the trailing vortices eventually destroyed? This question has three interrelated aspects: firstly, the formation of the horseshoe vortices and vortex rings in the initial stages of the motion; secondly, the mechanisms by which the trailing vortices develop instabilities and break into smaller segments; and, finally, the relationship between the existing analytical models of the behaviour of trailing vortices and the demise mechanisms.

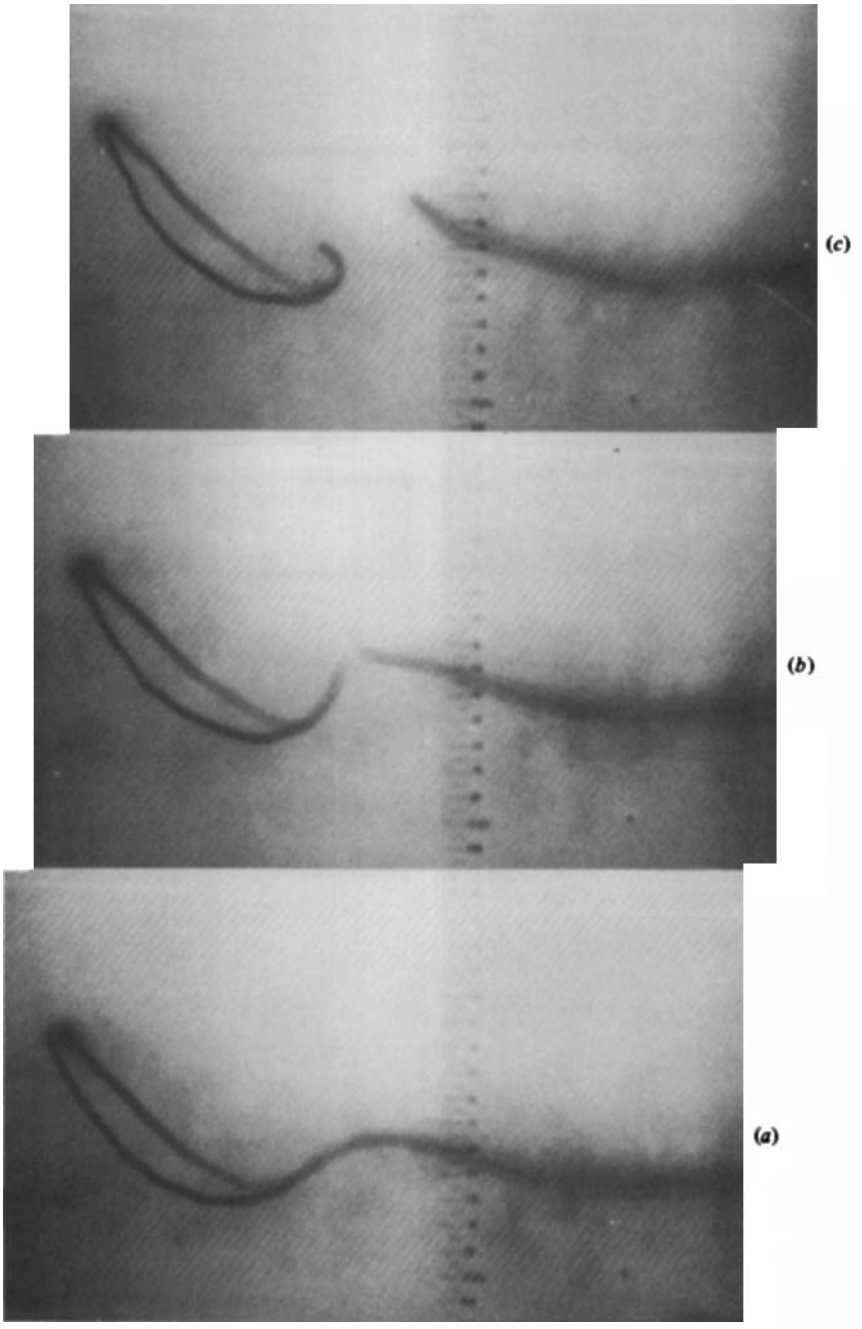

FIGURE 7. (*a*) Formation of the first horseshoe vortex; (*b*) linking of the vortices; (*c*) formation of the first vortex ring. Note that the vertical scales are lined up to show the lateral motion of the ring.

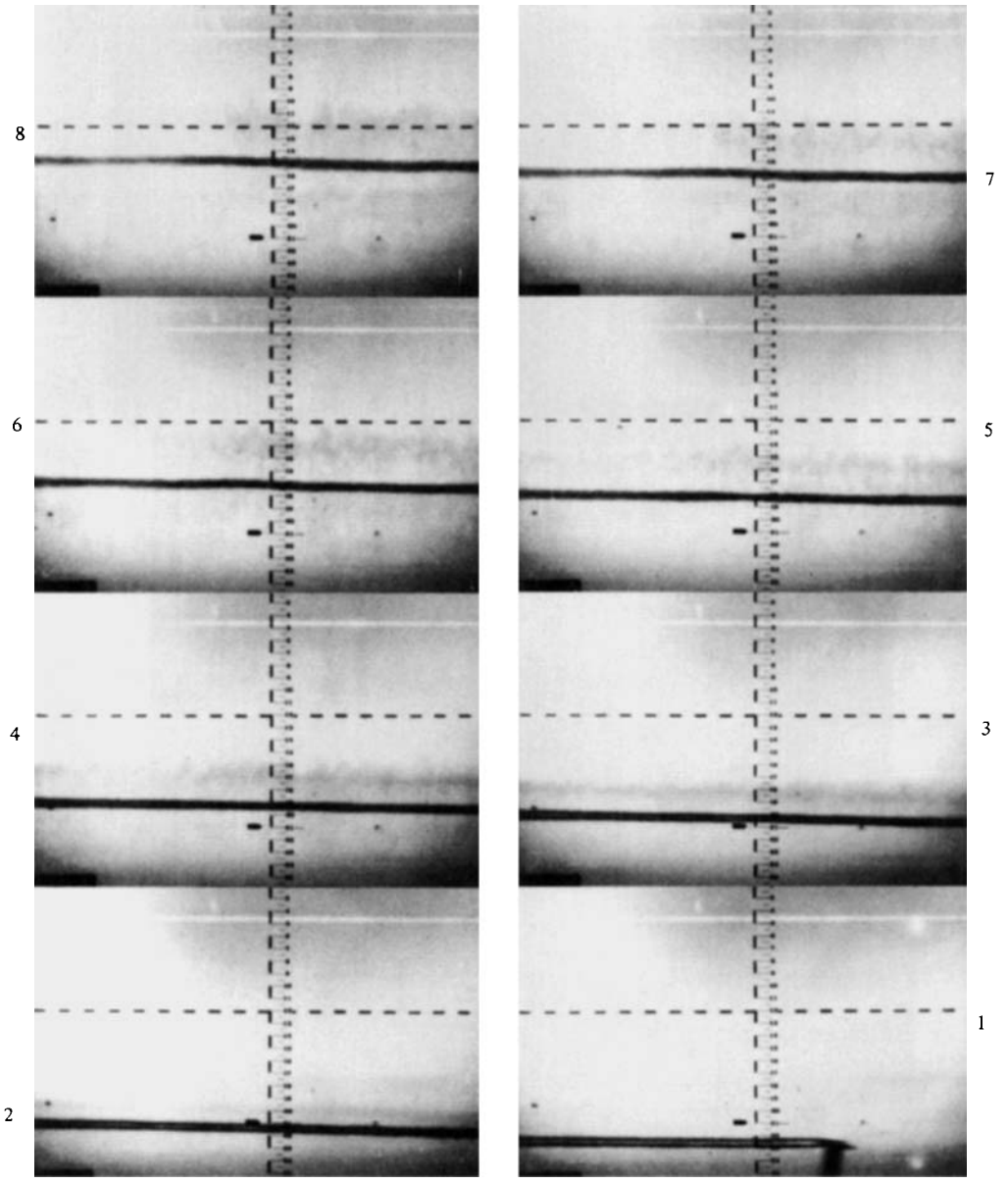

(*a*)

FIGURE 8. The development of Crow instability on vortices generated by a rectangular wing (NACA 0012).

4.1. *Horseshoe vortices and vortex rings*

As the lifting surface is set in motion impulsively from rest, the vorticity shed from the surface forms a so-called horseshoe vortex. Shortly after the formation of this vortex, linking occurs and the horseshoe vortex transforms into a vortex ring (see figure 7). The observations and measurements have shown that the vortex ring inclines itself at an angle of about 45° and undergoes complex transformations partly under the influence of self-induced velocities and partly due to the velocities induced

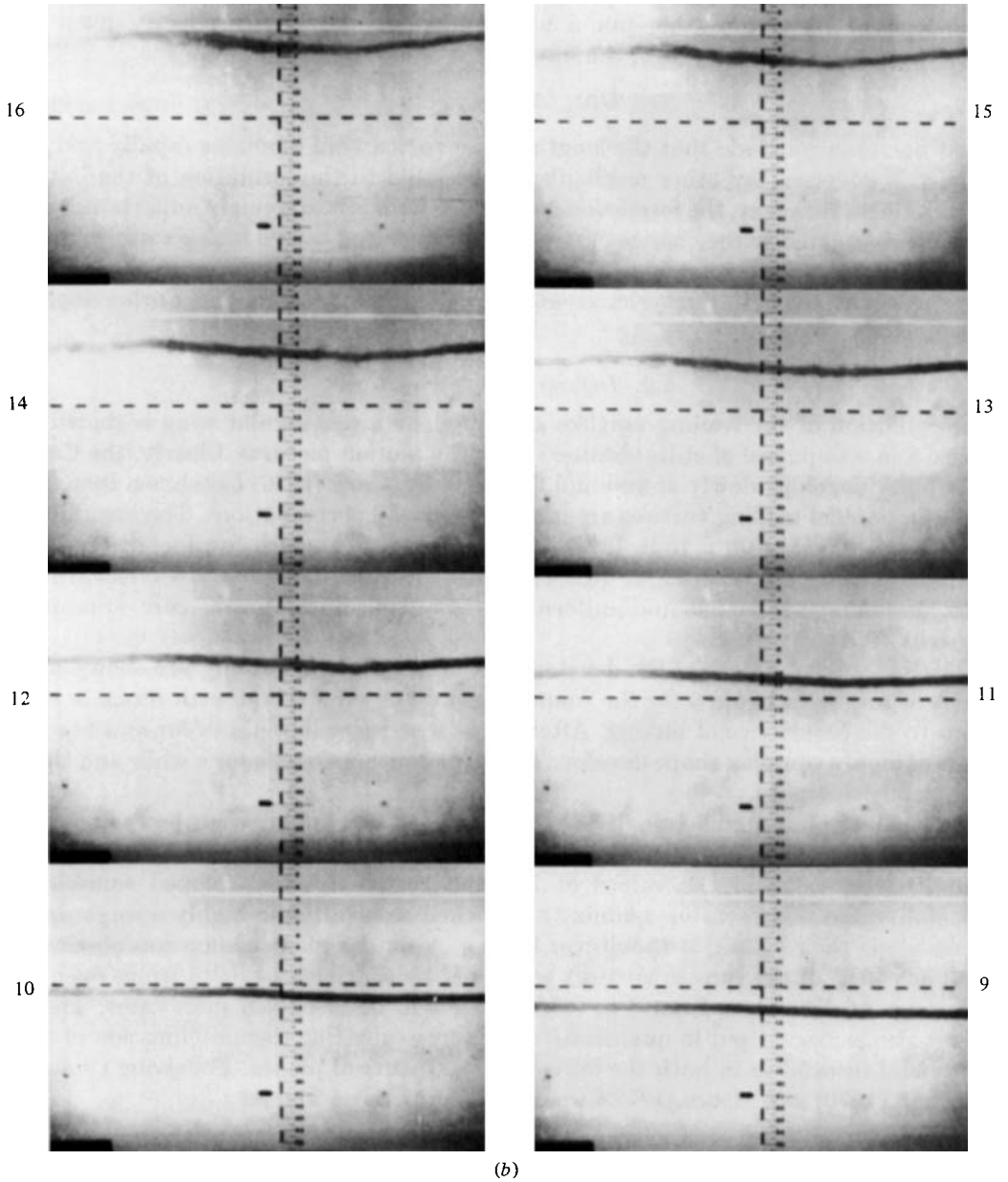

(*b*)

by the remainder of the trailing vortex. The non-uniformity of the velocities induced on the ring results in vortex stretching in addition to gross deformations due to Widnall instability (Widnall 1975).

Following the formation of the first ring, the end of the trailing vortices necessarily links and forms a new horseshoe vortex. This, in turn, results in a new vortex ring with similar consequences. Repeated experiments have shown that as many as four rings are formed. Each ring is different at birth and is subjected to different velocity fields subsequently. The distance as well as the time interval between the successive linkings have been determined and it was found that $\Delta x_n/\Delta t_n$ is nearly constant for

a given U (Δx_n is the horizontal distance between the nth link and the $(n-1)$th link and Δt_n is corresponding time difference). Comparing the linking velocity given by $\Delta x_n/\Delta t_n$ with the velocity U of the model, it was found that†

$$U\Delta t_n/\Delta x_n = 16\text{–}20. \tag{4.1}$$

Thus one may conclude that the length of the vortex trail increases rapidly and its demise is governed by other mechanisms unrelated to the formation of the initial vortex rings. However, the formation of the vortex rings is extremely important since it is closely related to the change of circulation generated by the lifting surface. Such a change may result either from the change of velocity and/or from the change of the angle of attack of the lifting surface and may precipitate and enhance other demise mechanisms.

4.2. *Demise of the vortex trail*

The evolution of the trailing vortices generated by a rectangular wing is shown in figure 8 in a sequence of stills obtained from the motion pictures. Clearly, the Crow instability develops slowly at first and then rapidly. Crow (1970) has shown that two initially parallel trailing vortices are unstable to small perturbations. The instability grows by a factor e in a time $1.21b_0/V_0$ in fixed planes which are inclined to the horizontal at an angle of about 48°. The most-unstable mode has a wavelength of $8.6b_0$ (assuming $r^* = 0.098$ and uniform vorticity distribution in the core – Spreiter & Sacks 1951).

The subsequent stages of the development of the Crow instability are shown in a series of frames in figure 9 for the round-edged delta wing. The fourth frame is just prior to the occurrence of linking. Afterwards, a series of linkings occur and vortex rings of highly complex shape develop. The rings continue to rise for a while and then completely dissipate.

In the data presented herein, the Crow instability and linking was observed in the trailing vortices for N^* smaller than about 0.75 for most of the runs with models with rounded edges. At higher values of N^*, the vortices first developed sinusoidal instability and then went on spinning about their axes (often in highly disorganized forms along their length) without ever linking. A similar phenomenon was observed in about 40 % of the runs in vortices generated by sharp-edged delta wings even in the range of N^* values from 0 to 0.75. These will be discussed more later. These observations may be put in quantitative form by evaluating the amplification of the sinusoidal instability in both the horizontal and vertical planes. Following Crow & Murman (1970) and Moore (1972), we define a growth parameter

$$\beta(t^*) = \frac{b_{\max}(t^*) - b_{\min}(t^*)}{b_{\max}(t^*) + b_{\min}(t^*)} = \beta(0)\,\mathrm{e}^{\alpha_h t^*}, \tag{4.2}$$

where $b_{\max}(t^*)$ represents the maximum vortex separation, $b_{\min}(t^*)$ the minimum vortex separation and α_h the rate of amplification in the horizontal plane. $\beta(t^*)$ is zero in the absence of perturbation, grows exponentially with t^* during the linear instability, and becomes unity when the vortices link at points of minimum separation.

† This ratio should not be confused with the ratio of the time $1.12b_0/V_0$ during which the sinusoidal instability grows by a factor e (Crow 1970), to the time $s/U = 0.36(AR/C_L)\,b_0/U$, during which the trailing vortices are considered to be essentially rolled up (Spreiter & Sacks 1951). Crow found that $(1.21b_0/V_0)/(s/U) = 26$.

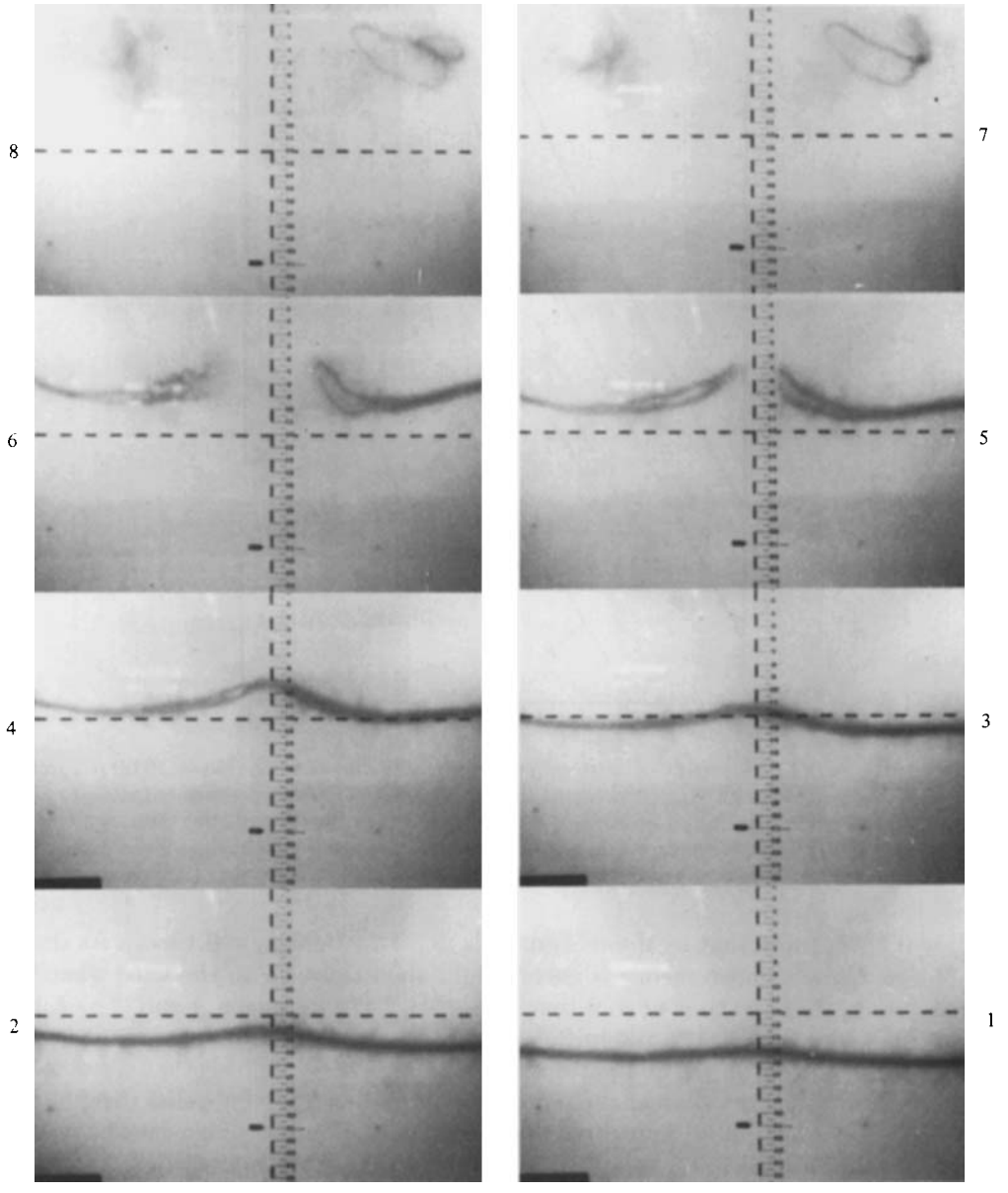

FIGURE 9. Subsequent stages of the Crow instability, linking of vortices, and the development of vortex rings.

Figure 10 is a plot of $\beta(t^*)$ as a function of t^*, in semilogarithmic coordinates, for seven different cases. Curves labelled A and B represent the calculations of Moore (1972), based on a numerical study of the finite-amplitude instability of the mutual interaction. Only the slope of these curves is determined by the analysis ($\alpha_h = 0.847$ according to the linear analysis of Crow). Their vertical position depends on the initial amplitude of the disturbance, i.e. on $\beta(0)$ for $N^* = 0$. Curve A is for an initial amplitude of $\beta(0) = [b_{max}(0) - b_{min}(0)]/b_0 = 0.10$ and curve B for $\beta(0) = 0.0552$. In both cases, the calculation was terminated when the vortices nearly touched, i.e. when

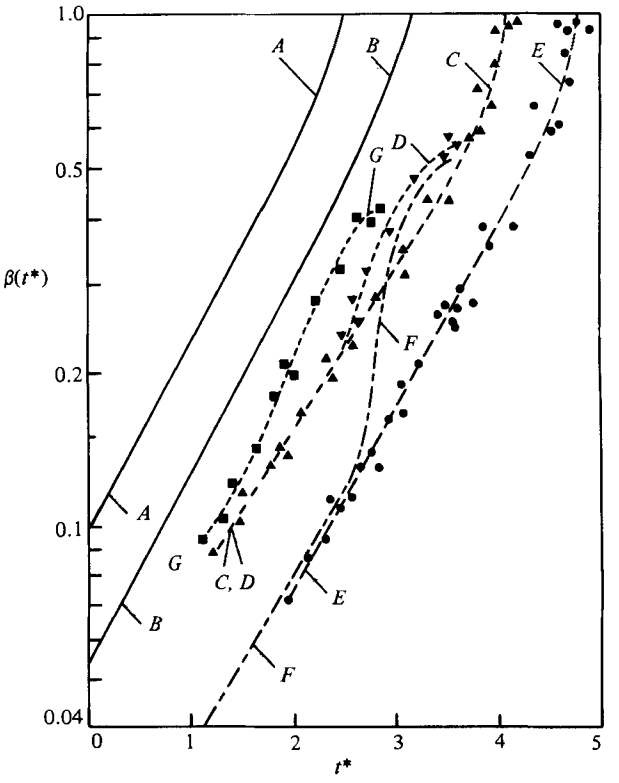

FIGURE 10. Growth rate versus t^*: A, with $\beta(0) = 0.1$; B, with $\beta(0) = 0.055$ (Moore 1972); C, present data with sharp-edged delta wings and vortex linking; D, present data with sharp-edged delta wings and no vortex linking (common linear regions of C and D are shown with the same symbol); E, present data with models with rounded rips; F, mean line through the flight data (Crow & Murman 1970); G, present data with sharp-edged models and $N^* = 0.50$.

$b_{\min} = 0.187b_0$ (note that in Moore's analysis $2r_c = 2 \times 0.098b_0 = 0.198b_0$). As shown by Moore, Crow's linear theory is surprisingly good right up to the time when the vortices link, t^* at the time of core touching ($t^* = 2.475$ for curve A and $t^* = 3.2$ for curve B) is very sensitive to the initial amplitude of the disturbances, and it is only through the 'cut-off' in the evaluation of the Biot–Savart integrals that the detailed structure of the vortex filament, particularly its radius and the radial distribution of vorticity and axial flow, influences the calculations. Similar conclusions have been reached by Widnall, Bliss & Salay (1971) and by Moore & Saffman (1972). According to Widnall *et al.*, who assumed an arbitrary distribution of swirl and axial velocities, the effect of axial velocity is to reduce the length of the most unstable of the long waves and to decrease slightly its amplification rate. Furthermore, their analysis predicted a slight decrease in α_h with increasing r^*.

Curves C and D in figure 10 show the results obtained with the sharp-edged delta wings. For t^* less than about 1.3, $b(t^*)$ remained nearly constant (the amplitude of the disturbances was less than about $0.05b_0$). The disturbances continued to grow in the linear range up to $t^* \approx 3.7$ (see curve C in figure 10) with a rate of amplification $\alpha_h \approx 0.74$. In approximately 30 % of the test runs with sharp-edged models, the vortices linked at $t^* \approx 4.1$, after going through an accelerated amplification under nonlinear effects in the range $3.7 < t^* < 4.1$. Subsequently, the distorted vortex rings continued to rise and the last vestige of the vortex trail disappeared at $t^* \approx 6.2$. In approximately

40 % of the tests,† the vortex pair became disorganized towards the end of the linear range ($t^* \approx 2.6$), and did not permit a meaningful evaluation of $\beta(t^*)$ beyond $t^* \approx 3.6$ (see curve D in figure 10 and the gradual broadening of the scatter in the data shown in figure 1 in the range $2.6 < t^* < 3.6$ on account of the disorganized vortices). For t^* larger than about 3.6, the D-type wake structure continued to rise to just about the same height as the C-type vortices and vortex rings. This is somewhat surprising. One would have expected a reduction in maximum height relative to the C-type vortices on the grounds that the disorganized form will enhance turbulence and energy dissipation.

The wavelength λ varied from run to run and from wave to wave in a given run. The analysis of the entire data with the sharp-edged models yielded $\lambda = (7.8 \pm 0.5)\, b_0$ for both the C- and D-type vortices in their linear range.

The curve E in figure 10 shows the results obtained with the models with rounded tips, corresponding to the data shown in figure 4. In the linear range, the data yielded $\alpha_h = 0.81$ and $\lambda = (8.2 \pm 0.4)\, b_0$. The vortices linked (in about 90 % of the runs) at $t^* \approx 4.7$, and the vortex rings completely disappeared at $t^* \approx 7.3$ (see figure 4, where the scatter in the data begins to increase at $t^* \approx 4$).

The steepness‡ of the sinusoidal disturbance was nearly identical in horizontal and vertical planes for $t^* < 4$, showing that the instability was confined to planes inclined at about 45° to the horizontal. This compares well with Crow's prediction of 48° in the linear range. Just prior to linking, however, the average value of the wave steepness was $b_{max}/2\lambda \approx 0.075$ in the horizontal plane and $H_{wv}/\lambda \approx 0.11$ in the vertical plane, showing that the plane‖ of instability rotated rapidly in the non-linear range from about 45° to about 55° relative to the horizontal. This result tends to confirm the calculations of Moore (1972), who found 56.5° for this angle.

The comparison of the relative positions of the curves C, D and E in figure 10 and of the data in figures 1 and 4 in the light of the analytical results of Widnall *et al.* (1971), regarding the relatively small effect of r^* and the type of distribution of swirl and axial velocities on α_h, lends support to the conjecture that the earlier inception of the Crow instability for models with sharp edges is due primarily to relatively higher intensity and scale of turbulence entrapped in the vortices during the roll-up process. Should this prove to be the case then the increase in r^* for the sharp-edged models is a consequence, as well as an indirect and integrated measure, of the increased diffusion of vorticity due to higher levels of turbulence.

The curve F in figure 10 is the normalized form of a flight data¶ (the only such data known to us) reported by Crow & Murman (1970) and later by Condit & Tracy (1971). The instability grew exponentially at first and then at an accelerated rate, until the wake became too disorganized to permit a meaningful evaluation of $\beta(t^*)$. The similarity between the curves D and F is striking but may be fortuitous in view of the widely different scales of the experiments.

The interaction of the sinusoidal instability with linear stratification proved to be extremely complex particularly for $N^* > 0.75$. The problem was further compounded

† In the remaining 30 % of the tests with sharp-edged models, core bursting occurred.

‡ Steepness is defined as $(b_{max} - b_{min})/2\lambda$ in the horizontal plane and as H_{wv}/λ in the vertical plane. H_{wv} is the wave height.

‖ No attempt was made to ascertain that the instability in the nonlinear range was in fact confined to a 'plane'.

¶ The 747 was in a takeoff configuration (flaps 10, gear up), $U = 83.3$ m/s, and at an altitude of 1493.5 m. The data was normalized with $V_0 = 8W/(\pi^3 B^2 \rho U)$ where W (the weight of the aircraft) = 2331000 N and $B = 59.65$ m. Note that V_0 was not given in the original data.

by the difficulty of making several experiments for a given N^* (normally a 10 min experiment required 6 h of preparation to achieve the desired stratification). For N^* smaller than about 0.75, the vortices first developed sinusoidal instability and then either linked and formed highly irregular shapes (often with models with rounded tips) or came to an almost full stop without ever linking (often with sharp-edged models). Subsequently, both forms of vortices have dissipated in about one-third of the time it took them to reach the particular states just described. Curve G in figure 10 shows the results obtained in two runs with sharp-edged models for $N^* = 0.50$. The change in α_h with t^* is attributed to the effects of the countersign vorticity generated at the boundary of the recirculation cell.

At higher values of N^*, the vortex pair developed sinusoidal instability but no linking. The wave steepness in the horizontal plane did not exceed 0.05. Then the vortices went on spinning until they were eventually destroyed. These observations are consistent with the development of countersign vorticity whose centroid is primarily below and outboard of the ascending vortex cores (Hecht, Bilanin & Hirsh 1981; Sarpkaya & Johnson 1982).

The last demise mechanism to be discussed is the vortex breakdown. When the axial velocity in a single vortex becomes nearly equal to the maximum tangential velocity at the edge of the core, the vortex undergoes an abrupt transition from supercritical to subcritical flow in axisymmetrical or spiral or double-helix form (Sarpkaya 1971).

Observations and measurements have shown that the trailing vortices in homogeneous as well as stratified medium survive the vortex breakdown and continue to rise. In fact, the maximum height reached by the vortices or their remnants was nearly the same, regardless of whether the instability resulted in linking or core bursting, at least in a homogeneous medium.

Figure 11 shows a few of the successive frames following the inception and growth of the vortex breakdown in one of the trailing vortices generated by the rectangular wing moving at angle of attack of $-12°$ ($N^* = 0$). About 30 % of the test runs with the sharp-edged models and about 10 % of the test runs with rounded models resulted in vortex breakdown. The axial velocity (as determined in a few cases through the observation in film of the methylene blue particles trapped in the core) was about $0.3U$ for the sharp-edged models and about $0.2U$ for the rounded models. The horizontal distance occupied by a single breakdown was approximately $4b_0$, i.e. about half the wavelength of the sinusoidal instability. The breakdown always occurred following the inception of Crow instability and at points of maximum separation of the filaments, as anticipated by Bilanin & Widnall (1973). The breakdown remained stationary (see figure 11) even when another breakdown occurred further upstream. Finally, the vortex filament downstream of the breakdown remained practically unaffected. The last two observations are in contradiction to those made on single vortices in a tube (Sarpkaya 1971). In other words, the vortex breakdown in trailing vortices does not signal a transition from supercritical to subcritical flow. It appears that what is commonly called vortex breakdown in trailing vortices is a somewhat different phenomenon and it would be more appropriate to call it 'core bulging and bursting'. However, the fact that it is strongly influenced by an adverse pressure gradient can easily be demonstrated by placing an axisymmetric streamlined body in the vicinity of the trailing vortices. Lastly, a series of breakdowns at desired locations along the trailing vortex can be generated by stretching thin wires across the tank at a height several b_0 from the model elevation. Such experiments have shown that each breakdown remains at where it is generated. It appears that much

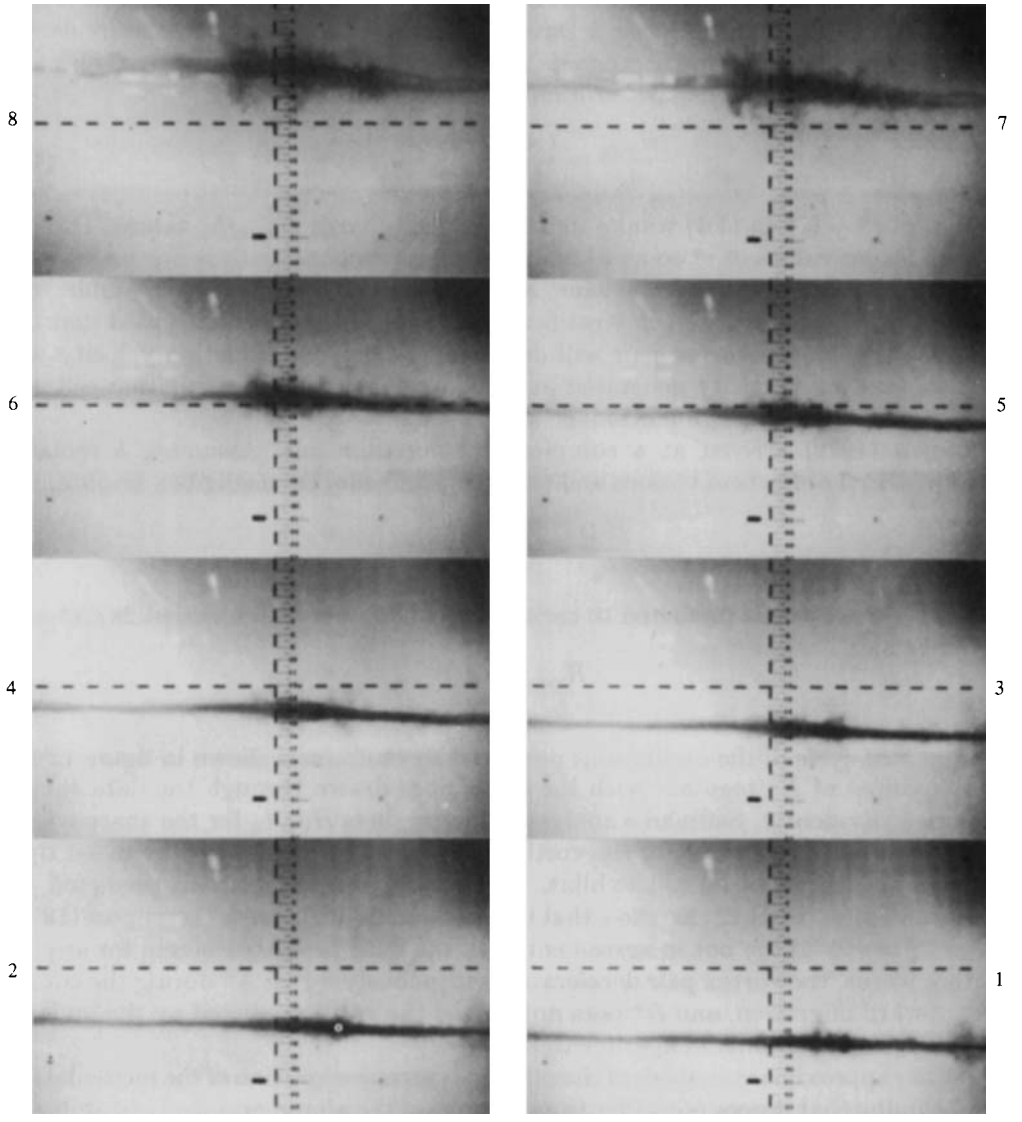

FIGURE 11. Evolution of core bulging and bursting in trailing vortices generated by a NACA-0012 wing.

additional work is needed to delineate the characteristics of core bulging and bursting in trailing vortices.

4.3. *Comparison of analytical and experimental results*

Scorer & Davenport (1970) determined the trajectory of the vortices in a stably stratified fluid by assuming the circulation to be a constant and by equating the rate of change of impulse of the vortex system to the buoyant force. Their analysis yielded

$$\frac{H(t)}{b_0} = \left(\frac{8\pi}{\sigma}\right)^{\frac{1}{2}} \frac{1}{N^*} \sinh\left(\left(\frac{\sigma}{8\pi}\right)^{\frac{1}{2}} N^* t^*\right), \tag{4.3}$$

where $\sigma = 11.3$ according to Saffman (1972). A plot of (4.3) is shown in figure 12 for representative values of N^*. Scorer & Davenport further assumed that the recirculation cell will cease to rise when the vortices annihilate each other by having their cores touch, i.e. $b_{\min} = 2r_c$.† This assumption resulted in

$$\frac{H_{\max}}{b_0} = \frac{1.492}{N^*}\left(\frac{1}{4r^{*2}} - 1\right)^{\frac{1}{2}}. \tag{4.4}$$

The use of $r^* = 0.1$ in (4.4) results in unrealistically large $H_{\max}/b_0$ values. The use of much larger values of r^* so as to match the experimental data is not warranted. Crow (1974) derived exactly the same set of equations from his theory under the assumption of vanishingly weak stratification. These two studies concluded that the distance between the vortex pair will decrease, the mutual induction velocity will increase, and the vorticity generated at the boundary of the recirculation cell will continuously drain through a drainage slot.

Saffman (1972) arrived at a completely different result. Assuming b remains constant and the effects of viscous and turbulent diffusion are negligible, he obtained

$$\frac{H(t)}{b_0} = \frac{1}{N^*}\sin N^* t^*. \tag{4.5}$$

Thus the vortex pair is predicted to oscillate up and down with a period $2\pi/N^*$ and an amplitude

$$\frac{H_{\max}}{b_0} = \frac{1}{N^*}. \tag{4.6}$$

The first half-cycle of the oscillations predicted by Saffman is shown in figure 12 for various values of N^* together with the mean lines drawn through the data shown in figure 5. Evidently, Saffman's analysis underpredicts $H(t)/b_0$ for the sharp-edged models. This is even more so for the vortices generated by models with rounded tips. Furthermore, the data do not exhibit, for any N^*, the cyclic trend predicted by Saffman. Figures 5 and 12 also show that the predictions of Scorer & Davenport (1970) and of Crow (1974) are not in agreement with the data presented herein for any t^*. In other words, the vortex pair decelerates continuously for all N^* during the course of its upward migration, and H^* does not exceed the value predicted by the inviscid theory within the limits of experimental accuracy.

Another approximate analysis of the ultimate vertical migration of the recirculation cell, assuming that it does not suffer from any one of the aforementioned instabilities, may be carried out by equating the initial kinetic energy to the final potential energy of the recirculation cell. This assumption and the use of $r^* = 0.1$ yields (Hecht *et al.* 1980; Sarpkaya & Johnson 1982)

$$\frac{H_{\max}}{b_0} = \frac{2.39}{N^*}. \tag{4.7}$$

Equations (4.4), (4.6) and (4.7) yield infinitely large values for $H_{\max}/b_0$ for $N^* = 0$. Furthermore, they do not account for any of the known demise mechanisms. The particular dependence of $H_{\max}/b_0$ on N^* strongly suggests that the phenomena such as turbulence, entrainment and detrainment of the recirculation cell, Crow instability,

† The reader is warned that the core radii r_c used here and in Widnall *et al.* (1971) differ from each other as well as from the one used in the rest of this paper because of the differences in vorticity distribution.

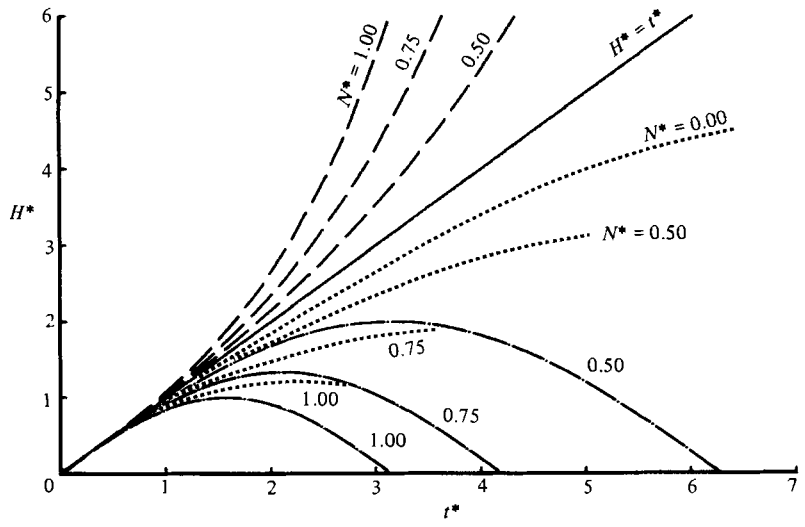

FIGURE 12. Comparison of the theoretical and experimental results: ———, Scorer & Davenport (1970) and Crow (1974); ———, Saffman (1972); – – – – –, mean lines drawn through the present data shown in figure 5.

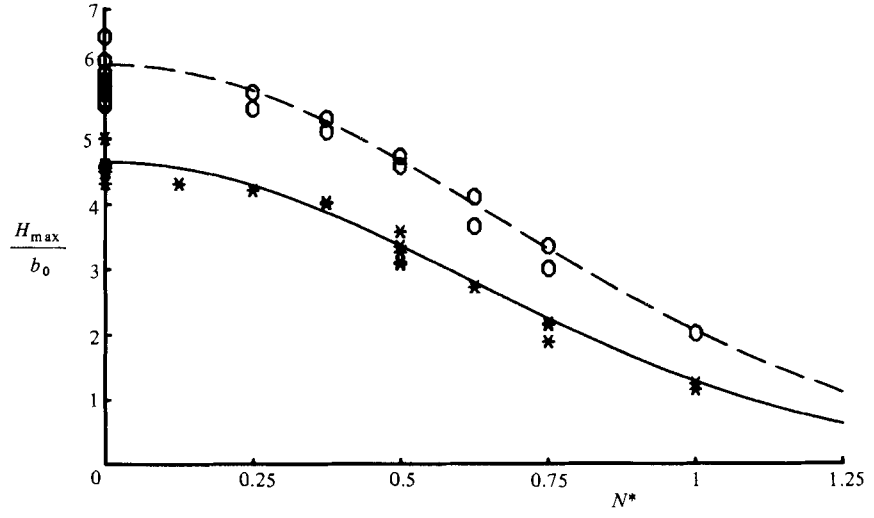

FIGURE 13. Maximum rise of vortices generated by: ○, wings with rounded tips; *, wings with sharp-edged tips. Dashed and solid lines represent the mean lines drawn through the data.

and the vortex bursting play far more complex roles than can be quantified in a simple approximate analysis. The experimental data for H_{max}/b_0 are shown in figure 13. Clearly, the vortices have a self-limiting effect on their rise even in homogeneous medium. The stratification imposes a further limitation on H_{max}/b_0. In all cases, about one-third of the maximum rise takes place after the onset of linking of vortices or after the bursting of the vortex core (see figure 10). Thus it is not a simple matter to determine H_{max}/b_0 with great precision, even experimentally. Since the vortex wake resulting from the Crow instability alone (vortex rings or disorganized vortex filaments) is not the same as that followed by vortex bursting, one does expect

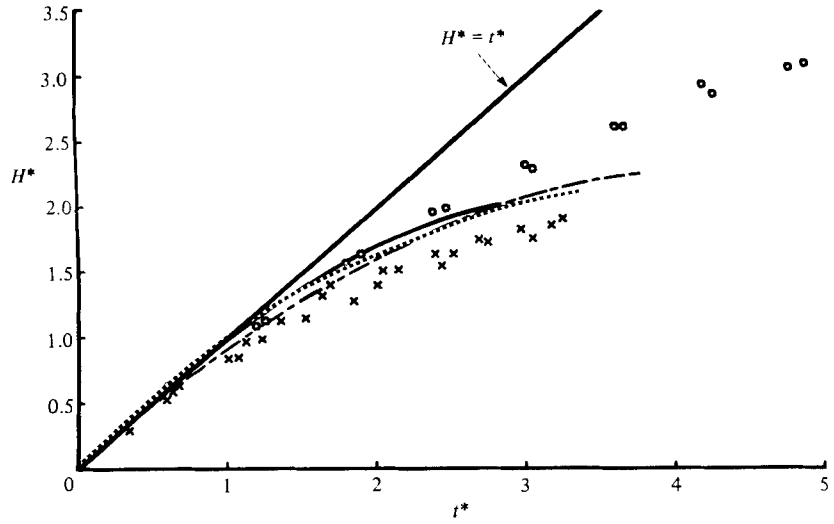

FIGURE 14. Comparison of experimental data and numerical prediction: present data: ○, $N^* = 0.50$; ×, $N^* = 0.75$. ----------, Burnham *et al.* data (1978); ——, numerical analysis (Hecht *et al.* 1981); ————, present data after interpolation (all for $N^* = 0.67$).

considerable scatter in H_{max}/b_0. This is evidenced by the data shown in figure 13, particularly for $N^* = 0$.†

In an effort to account for the real-fluid effects, such as turbulence, on aircraft vortex descent in stratified fluids, Hecht *et al.* (1980, 1981) developed a finite-difference computer code which solves the two-dimensional, unsteady mean and ensemble-averaged Reynolds stress equations of fluid motion based on a second-order-closure turbulence model. The results of the code were used as a guide in interpreting vortex-pair behaviour in a stratified atmosphere, and the role of turbulence in influencing this behaviour. Hecht *et al.* (1981) obtained close agreement between the calculated and observed behaviour of a turbulent vortex descending in a stable stratification (run 8 of Burnham *et al.* 1978).

Figure 14 shows our data for two values of N^* (obtained with the sharp-edged wings as shown in figure 5), the mean line drawn through the flight data,† and the corresponding numerical predictions of Hecht *et al.* (1981). The agreement between these results for $N^* = 0.67$ is rather surprising for a number of reasons. (i) Our data and those of Burnham *et al.* are obtained with bodies, entirely different in shape and size, operating under widely different flow conditions (e.g. circulation for the test aircraft was about 630 m^2/s as compared with 0.035 m^2/s for the present data shown

† In figure 13 the data for sharp-edged models may be approximated by $H_{max}/b_0 = 4.64\exp[-1.3(N^*)^2]$, and the data for models with rounded tips by $H_{max}/b_0 = 6.10\exp[-1.1(N^*)^2]$. The use of these expressions is not warranted beyond the range of parameters encountered in the present experiments.

† In reducing the flight data of Burnham *et al.*, H was measured from the initial altitude of the aircraft (i.e. 244 m) and not from the position the vortex pair occupied at 10 s after passage of the generating aircraft. The values assigned to the controlling parameters were identical with those used by Hecht *et al.* (1981), viz $N = 0.0265$ rad/s, $b_0 = 50$ m, $V_0 = 1.98$ m/s, and thus $N^* = 0.67$. Note that the data of Burnham *et al.* fall above the ideal line, $H^* = t^*$, in the range $0 < t^* < 1$ in figure 14. The uncertainty in field tests, particularly at small times, prevents us from interpreting the noted increase in vortex speed as confirmation of the theoretical predictions of Scorer & Davenport (1970) and of Crow (1974), at least for $t^* < 1$ (see also figure 12).

in figure 14. Γ/ν for the flight data was about three orders of magnitude and the chord-based Reynolds number was about two orders of magnitude larger than those for the laboratory data). (ii) There is no reason to assume that the distributions of vorticity, turbulence, and the axial and radial velocities were similar. (iii) The two-dimensional turbulent flow simulation of Hecht *et al.* does not deal with large-scale three-dimensional instabilities such as the Crow instability and vortex bursting.

There is one notable exception to the above remarks: the behaviour of the vortex pair in the three studies is not radically different. Burnham *et al.* noted that in the particular test flight (run 8) the vortex pair developed 'sinuous instability' and then a number of anomalies such as the disappearance of the velocity dips marking the vortex core. They have also noted that 'some of the anomalies may have been related to a burst'. In our experiments, the vortex pair always developed sinusoidal instability but did not always link. In fact, in about 40 % of the runs in homogeneous fluid and in a larger percentage of runs in stratified fluid, the sinusoidal instability in the vortices generated by the sharp-edged wings did not culminate in linking. Instead, as noted before, the vortex pair became highly disorganized along its length and either developed a cascade of bursts or went on spinning about their axes under the influence of countersign vorticity generated at the boundary of the recirculation cell. In the numerical simulation by Hecht *et al.* the vortices decayed slowly during descent and retained appreciable circulation after descent has stopped at $t^* = 2.8$. Thus it appears that the development of a mild sinusoidal instability in the earlier stages of the evolution of the vortices in both the laboratory and flight experiments does not significantly affect the lifespan of the vortex pair, primarily owing to the absence of linking. Even though in a homogeneous medium the vortex pair rises to about the same height regardless of whether it has undergone linking or bursting, there is no way to ascertain that the same will hold true for a vortex pair ascending in a highly stratified fluid, simply because the vortices will not link. On the other hand, the occurrence of core bursting, following a mild sinusoidal instability, enhances turbulence, lending credibility to the conjecture that the lifespan of the vortices under consideration is governed primarily by turbulence, countersign vorticity, and the entrainment and detrainment of vorticity from the recirculation cell.

In our experiments, the last data point represents the state of total dissipation of the vortex pair (at $t^* \approx 3.8$, by interpolation). The rise of the vortex pair in the range $2.8 < t^* < 3.8$ is rather small, tending to confirm the finding by Hecht *et al.* that the vortices retain appreciable circulation after descent has stopped at $t^* = 2.8$. The data of Burnham *et al.* stop at $t^* = 3.3$, not because the vortices were observed to have completely dissipated but because the measurements were terminated after 83 s. Thus the vortex pair in the three studies might have completely dissipated at about the same normalized time without gaining appreciable additional height beyond $t^* = 2.8$.

Even though we are unable to explain the agreement between the results of the three studies for $N^* = 0.67$, it appears that the lifespan of the vortices is governed primarily by large-scale instabilities for small values of N^* and by turbulence and the attendant consequences of countersign vorticity for large values of N^*. In the latter case, the judicious selection of the turbulent scale for use in numerical simulations is very important and deserves additional work. An experimental investigation along these lines is currently under way.

5. Concluding remarks

Is the lifespan of the trailing vortices always controlled by large-scale instabilities excited by turbulence? Our observations and measurements show that, in a weakly stratified medium, linking of the vortices and/or the cascade of core bursts are indeed primarily responsible for the destruction of the vortex pair. In this process, the role of the ever-present turbulent diffusion becomes paramount after the onset of the said instabilities. In a strongly stratified medium, the amplitude of the sinusoidal instability remains relatively small and the vortices do not link. In this case, the level of initial turbulence generated by the vortex pair, additional turbulence generated by core bursting, and the countersign vorticity generated at the boundaries of the recirculation cell determine the lifespan of the vortices even in a medium otherwise free from turbulence. The numerical simulations by Hecht *et al.* (1981) for $N^* = 0.67$ tend to support this view. A precise demarcation of the boundaries of weak and strong stratification in terms of N^* and the initial level of turbulence is not yet possible. There may even exist an intermediate stratification for which the sinusoidal instability, occasional linking, core bursting, and turbulent diffusion play equally important roles throughout the rise and demise of the vortices.

The comparison of flight data and the numerical predictions of Hecht *et al.* with the present data for $N^* = 0.67$ led to unexpected and largely unaccounted for agreement.

The suitability of a towing tank in conducting controlled laboratory experiments with trailing vortices and the importance of t^*, N^*, and the tip-shape of the test models (in determining the initial turbulence level and the core size) have been shown either directly or indirectly throughout the paper.

The comments and suggestions of the referees are sincerely appreciated. The author cannot adequately acknowledge all who have helped to germinate the ideas which resulted in the present paper, but would like appreciatively mention Dr Arthur J. Bruckheim (Program Manager) and Professors Steven C. Crow and Sheila E. Widnall. Thanks are also due Major Christos Striftos, Lt Steven K. Johnson, Lt Cavit Turkmen, and Lt Dan Simons. A special note of thanks is extended to Mr Jack McKay for his most skilful and dedicated work in the construction and smooth operation of the test facilities and models.

REFERENCES

Baker, G. R., Barker, S. J., Bofah, K. K. & Saffman, P. G. 1974 Laser anemometer measurements of trailing vortices in water. *J. Fluid Mech.* **65**, 325–336.

Barker, S. J. & Crow, S. C. 1977 The motion of a two-dimensional vortex pair in ground effect. *J. Fluid Mech.* **82**, 659–671.

Bartlett, G. E. & Vidal, R. J. 1955 Experimental investigation of influence of edge shape on the aerodynamic characteristics of low aspect ratio wings at low speeds. *J. Aero. Sci.* **22**, 517–534.

Bilanin, A. J. & Widnall, S. E. 1973 Aircraft wake dissipation by sinusoidal instability and vortex breakdown. *AIAA Paper* 73–107.

Burnham, D. C., Hallock, J. N., Tombach, I. H., Brashears, M. R. & Barber, M. R. 1978 Ground based measurements of a B-747 aircraft in various configurations. *US Dept of Transportation Rep.* FAA-RD-78-146.

Condit, P. M. & Tracy, P. W. 1971 Results of the Boeing Company wake turbulence test program. In *Aircraft Wake Turbulence and its Detection*, pp. 489–492. Plenum.

Crow, S. C. 1970 Stability theory for a pair of trailing vortices. *AIAA J.* **8**, 2172–2179.

CROW, S. C. 1974 Motion of a vortex pair in a stably stratified fluid. *Poseidon Research Rep.* no. 1.

CROW, S. C. & MURMAN, E. M. 1970 Trailing-vortex experiments at Moses Lake. *Boeing Scientific Research Labs, Seattle, Wash., Communication* 009.

DONALDSON, C. DUP. & BLANIN, A. J. 1975 Vortex wakes of conventional aircraft. *AGARDograph* AGARD-AG-204.

ELLE, B. J. 1958 An investigation at low speed of the flow near the apex of thin Delta wings with sharp leading edges. *ARC R & M* no. 3176.

HALLOCK, J. N. (ed.) 1977 *Proc. Aircraft Wake Vortices Conf.* Natl Tech. Info. Services, Springfield, VA 22161.

HALLOCK, J. N. & EBERLE, W. R. (eds.) 1977 Aircraft wake vortices: a state-of-the-art review of the United States R & D program. *Transportation Systems Center, Cambridge, MA. Rep.* FAA-RD-77-23.

HECHT, A. M., BILANIN, A. J. & HIRSH, J. E. 1981 Turbulent trailing vortices in stratified fluids. *AIAA J.* **19**, 691–698.

HECHT, A. M., BILANIN, A. J., HIRSH, J. E. & SNEDEKER, R. S. 1980 Turbulent vortices in stratified fluids. *AIAA J.* **18**, 738–746.

HOERNER, S. 1958 *Fluid-Dynamic Drag.* Published by the author, Midland Park, NJ.

LAMB, H. 1945 *Hydrodynamics*, 6th edn. Dover.

MOORE, D. W. 1972 Finite amplitude waves on aircraft vortices. *Aero. Q.* **23**, 307–314.

MOORE, D. W. & SAFFMAN, P. G. 1972 The motion of a vortex filament with axial flow. *Phil. Trans. R. Soc. Lond.* A **272**, 403–429.

OLSEN, J. H., GOLDBURG, A. & ROGERS, M. (eds.) 1971 *Aircraft Wake Turbulence and its Detection.* Plenum.

PANTON, R. L., OBERKAMPF, W. L. & SOSKIC, N. 1980 Flight measurements of a wing tip vortex. *J. Aircraft* **17**, 250–259.

SAFFMAN, P. G. 1972 The motion of a vortex pair in stratified atmosphere. *Stud. Appl. Math.* **2**, 107–119.

SARPKAYA, T. 1971 On stationary and travelling vortex breakdowns. *J. Fluid Mech.* **45**, 545–559.

SARPKAYA, T. & JOHNSON, S. K. 1982 Trailing vortices in stratified fluids. *Naval Postgrad. School Rep.* NPS-69-82-003.

SCORER, R. S. & DAVENPORT, L. J. 1970 Contrails and aircraft downwash. *J. Fluid Mech.* **43**, 451–464.

SPREITER, J. R. & SACKS, A. H. 1951 The rolling-up of the trailing vortex sheet and its effect on the downwash behind wings. *J. Aero. Sci.* **18**, 21–33.

TOMASSIAN, J. D. 1979 The motion of a vortex pair in a stratified medium. Ph.D. thesis, UCLA.

WIDNALL, S. E. 1975 The structure and dynamics of vortex filaments. *Ann. Rev. Fluid Mech.* **7**, 141–165.

WIDNALL, S. E., BLISS, D. B. & SALAY, A. 1971 Theoretical and experimental study of the stability of a vortex pair. In *Aircraft Wake Turbulence and Its Detection*, pp. 305–338. Plenum.